

Proton Spin Structure in the Resonance Region

F. R. Wesselmann,^{1,2} K. Slifer,¹ S. Tajima,¹ A. Aghalaryan,³ A. Ahmidouch,⁴ R. Asaturyan^{†,3} F. Bloch,⁵ W. Boeglin,⁶ P. Bosted,⁷ C. Carasco,⁵ R. Carlini,⁷ J. Cha,⁸ J. P. Chen,⁷ M. E. Christy,⁹ L. Cole,⁹ L. Coman,⁶ D. Crabb,¹ S. Danagoulian,⁴ D. Day,¹ J. Dunne,⁸ M. Elaasar,¹⁰ R. Ent,⁷ H. Fenker,⁷ E. Frlez,¹ L. Gan,¹¹ D. Gaskell,⁷ J. Gomez,⁷ B. Hu,⁹ M. K. Jones,⁷ J. Jourdan,⁵ C. Keith,⁷ C. E. Keppel,⁹ M. Khandaker,² A. Klein,¹² L. Kramer,⁶ Y. Liang,⁹ J. Lichtenstadt,¹³ R. Lindgren,¹ D. Mack,⁷ P. McKee,¹ D. McNulty,¹ D. Meekins,⁷ H. Mkrtchyan,³ R. Nasseripour,⁶ I. Niculescu,⁷ K. Normand,⁵ B. Norum,¹ D. Pocanic,¹ Y. Prok,¹ B. Raue,⁶ J. Reinhold,⁶ J. Roche,⁷ D. Rohe,⁵ O. A. Rondón,¹ N. Savvinov,¹⁴ B. Sawatzky,¹ M. Seely,⁷ I. Sick,⁵ C. Smith,¹ G. Smith,⁷ S. Stepanyan,³ L. Tang,⁹ G. Testa,⁵ W. Vulcan,⁷ K. Wang,¹ G. Warren,^{5,7} S. Wood,⁷ C. Yan,⁷ L. Yuan,⁹ J. Yun,¹⁵ M. Zeier,¹ and H. Zhu¹

(Resonance Spin Structure Collaboration)

¹University of Virginia, Charlottesville, Virginia 22903

²Norfolk State University, Norfolk, Virginia 23504

³Yerevan Physics Institute, Yerevan, Armenia

⁴North Carolina A&T State University, Greensboro, North Carolina 27411

⁵Universität Basel, CH-4056 Basel, Switzerland

⁶Florida International University, Miami, Florida 33199

⁷Thomas Jefferson National Accelerator Facility, Newport News, Virginia 23606

⁸Mississippi State University, Mississippi State, Mississippi 39762

⁹Hampton University, Hampton, Virginia 23668

¹⁰Southern University at New Orleans, New Orleans, Louisiana 70126

¹¹University of North Carolina, Wilmington, North Carolina 28403

¹²Old Dominion University, Norfolk, Virginia 23529

¹³Tel Aviv University, Tel Aviv, 69978 Israel

¹⁴University of Maryland, College Park, Maryland 20742

¹⁵Virginia Polytechnic Institute & State University, Blacksburg, Virginia 24061

(Dated: March 30, 2007)

We have examined the spin structure of the proton in the region of the nucleon resonances ($1.085 \text{ GeV} < W < 1.910 \text{ GeV}$) at an average four momentum transfer of $Q^2 = 1.3 \text{ GeV}^2$. Using the Jefferson Lab polarized electron beam, a spectrometer, and a polarized solid target, we measured the asymmetries A_{\parallel} and A_{\perp} to high precision, and extracted the asymmetries A_1 and A_2 , and the spin structure functions g_1 and g_2 . We found a notably non-zero A_{\perp} , significant contributions from higher-twist effects, and only weak support for polarized quark-hadron duality.

PACS numbers: 13.40.Gp, 13.88.+e, 14.20.Dh

Ever since the first polarized EMC experiment found that the proton's spin is not fully carried by its valence quarks [1], the nucleon spin structure has been studied extensively, for example at SLAC [2], CERN [3], and DESY [4]. The main focus has been on kinematics in the deep inelastic scattering (DIS) region and with large momentum transfer (high Q^2) where observations can be readily interpreted in a perturbative QCD framework. In more recent years, lower energy regimes ($Q^2 \sim 1 \text{ GeV}^2$) have grown in importance, where the transition from the asymptotically free to the bound configuration of the quarks can be probed. Evaluating the requisite moments of the spin structure functions requires data or model dependent extrapolations, up to parton momentum fraction $x = 1$, where the electromagnetic scattering probe interacts with the proton as a whole, including the kinematic region dominated by nucleon resonances.

The new experimental focus on the larger x and lower Q^2 regimes so far has been concentrated on longitudinal polarization as the dominant, and technically more accessible, component. This has limited investigations to the spin structure function g_1 , which represents the charge-weighted quark helicity distributions. Due to the success of DIS interpretations based on the naïve parton model, which is limited to longitudinal spin components, little emphasis has been placed on transverse spin studies. In contrast, the operator product expansion (OPE) approach to QCD includes transverse spin starting from leading twist [5, 6] and is applicable at all kinematics. Since each higher order of twist, interpretable as increased correlation between partons, adds another $1/Q$ term, higher twist contributions should be more prominent at low Q^2 . Although transverse spin is suppressed in DIS at leading twist, thus motivating the twist-2 WW approximation [7]

[†]deceased.

$$g_2^{\text{ww}}(x, Q^2) = -g_1(x, Q^2) + \int_x^1 g_1(y, Q^2) \frac{dy}{y}, \quad (1)$$

twist-3 should contribute significantly to g_2 . The OPE relates the twist-3 matrix element d_2 , which represents quark-gluon correlations, to the third moments of g_1 and g_2 [6],

$$d_2 = 3 \int_0^1 x^2 (g_2 - g_2^{\text{ww}}) dx = \int_0^1 x^2 (2g_1 + 3g_2) dx, \quad (2)$$

permitting comparison with QCD lattice calculations, and thus providing a clean test of the theory.

Also, the phenomenon of quark-hadron duality [8] has captured much interest [9, 10, 11, 12, 13]. This concept connects the perturbative QCD description of quarks and gluons to the hadronic description at lower energies. Whereas global duality relates the entire resonance region to extrapolations of the asymptotic structure functions, local duality relates the extrapolated quantities to restricted resonance regions. Both have been observed in unpolarized scattering [14], but precision measurements of the spin structure functions in the resonance region are needed to determine whether they also display duality. If local duality, as first seen by Bloom and Gilman [8], were observed for g_1 , this would not only demonstrate its universal, rather than accidental nature [15], but it could also serve to justify extrapolations. The potential usefulness of the latter for the determination of the moments increases at low Q^2 , where the resonances extend over wider ranges of x than at high Q^2 .

Experiment E01-006 was conducted in Hall C of the Thomas Jefferson National Accelerator Facility by the Resonance Spin Structure (RSS) collaboration. Utilizing established procedures and equipment, we have measured the asymmetries A_{\parallel} and A_{\perp} in the scattering of polarized electrons off a polarized proton target. These asymmetries are defined as the dimensionless, relative difference between the cross sections with parallel and anti-parallel (or perpendicular and anti-perpendicular) alignment of the proton and the electron spins. Focusing exclusively on the hadronic vertex, we are left with the virtual photon asymmetries A_1 and A_2 , which are functions of the virtual photon's four-momentum-squared $-Q^2$ and the invariant mass W of the final state. Without a measurement of A_{\perp} , this step would require the use of a model or a sweeping assumption. Further, switching from an external scattering view to an internal structure interpretation, we can obtain the spin structure functions $g_1(x, Q^2)$ and $g_2(x, Q^2)$, where Q^2 is interpretable as the energy scale set by the probe and, in DIS, x represents the fraction of the proton momentum carried by the constituent the probe interacted with. The exact relation between these quantities, and other relevant definitions, can be found in Sec. II of Ref. [2] or in Sec. 2.1 of Ref. [9].

The experiment used Jefferson Lab's continuous, polarized electron beam with energy of 5.755 GeV and a nominal current of 100 nA. The beam polarization was measured by a Møller polarimeter [16] installed upstream of the target, and the beam helicity was flipped at 30 Hz on a pseudo-random basis.

Frozen $^{15}\text{NH}_3$, in 1–2 mm fragments, was used as the proton target in the University of Virginia apparatus [17] in which a ^4He evaporation refrigerator at 1 K coupled with a 5 T polarizing magnet created a stable polarization environment. The polarization population enhancement was achieved via microwave pumping (dynamic nuclear polarization) and measured by an NMR system using pickup coils embedded in the target material. For the A_{\perp} measurement, the entire target apparatus was rotated by 90° in the scattering plane. About equal amounts of data were taken with each polarization direction, flipping the nuclear spins by adjusting the microwave frequency, to reduce systematic effects. To maintain uniform polarization in the bulk target material, the beam was continually moved across the face of the target in a 1 cm maximum radius spiral raster pattern around the beam axis. This extra degree of freedom required a dedicated beam position monitor [18] for accurate event reconstruction.

Scattered electrons were detected using the High Momentum Spectrometer (HMS), positioned at a scattering angle of 13.15° . Two different HMS momentum settings were used, 4.078 and 4.703 GeV, to cover the desired wide range in W , resulting in $0.8 < Q^2 < 1.4 \text{ GeV}^2$. A detector package consisting of hodoscope planes, wire chambers, a gas Čerenkov counter, and a lead glass calorimeter allowed for particle identification and measurement of the event kinematics. A more detailed description of the apparatus and technique can be found in Ref. [19].

Approximately 160 million scattering events were recorded on the proton target, resulting in highly precise determinations of the parallel and perpendicular asymmetries. These are obtained from observed raw event counting asymmetries which are scaled to 100% polarization and corrected for contamination from radiative and dilution processes:

$$A_{\parallel, \perp} = \frac{1}{f C_N P_b P_t f_{RC}} \times \frac{N^- - N^+}{N^- + N^+} + A_{RC} \quad (3)$$

Here, N^\pm is the charge corrected observed yield for the parallel (perpendicular) and anti-parallel (anti-perpendicular) spin alignment, respectively. P_b and P_t are the beam and target polarizations, f is the dilution factor, C_N is a small ^{15}N nuclear polarization correction, and f_{RC} and A_{RC} are radiative corrections.

The corrected asymmetries A_{\parallel} and A_{\perp} are shown in Fig. 1; A_{\perp} is notably non-zero. The average proton polarization was 62% (70%), and the beam polarization was 71% (66%) during the parallel (perpendicular) running.

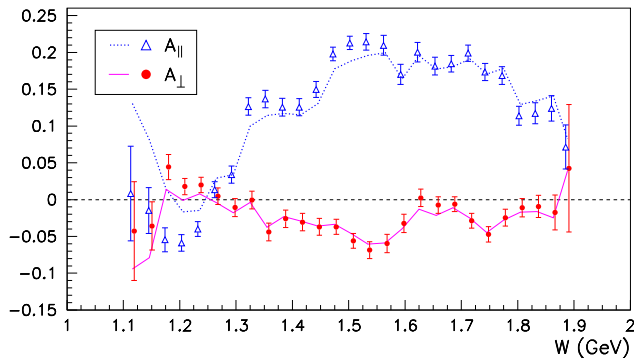


FIG. 1: Our measured asymmetries A_{\parallel} and A_{\perp} , fully corrected (points) and without radiative corrections (curves).

For the parallel alignment, the product $P_b \times P_t$ was derived by normalizing the measured elastic asymmetry [19] to the known value, resulting in better accuracy than achievable from direct measurements. In the perpendicular case, the limited knowledge of the elastic asymmetry made the direct measurement of P_b and P_t the better choice. The systematic errors are summarized in Table I, highlighting the lack of models and data for perpendicular radiative corrections.

The dilution factor represents the fraction of events that truly scattered from a polarized proton in the target. It was determined from the ratio of free proton to total target rates calculated via a Monte Carlo simulation which had been matched to calibration data acquired specifically for this purpose. The QFS parameterization [20], modified to improve agreement with our data, was used as input for the Born inelastic cross sections for $A \geq 3$ nuclei. Fits to Hall C inelastic $e-p$ data [21] were used for the H contribution. The unpolarized structure function F_1 and the ratio R of the longitudinal to transverse cross sections are derived from the same fits [21, 22]. The uncertainty in these cross sections was the dominant source of systematic error for the dilution correction.

Convoluting radiative prescriptions with models of the resonance region, the elastic peak, and our target, we obtained radiated cross sections and asymmetries. The external radiative corrections were determined using the procedure established in [23], while the POLRAD software [24] was used to determine the internal radiative

TABLE I: Averaged systematic errors in the asymmetries.

Error Source	A_{\parallel}	A_{\perp}
Target Polarization	} 1.1 %	2.9 %
Beam Polarization		1.3 %
Dilution Factor	4.9 %	4.9 %
Radiative Corrections	2.7 %	12.9 %
Kinematic Reconstruction	0.4 %	0.4 %

corrections. The resonance fit model was iteratively improved, until the radiated values matched our experimental data. The model then trivially provided the corrections to our measurements, with f_{RC} accounting for the radiative dilution from the elastic tail and A_{RC} for all other influences.

We extract the virtual photon asymmetries A_1 and A_2 , shown in Fig. 2, from the corrected physics asymmetries A_{\parallel} and A_{\perp} , using only R as model dependent input. The spin structure functions g_1 and g_2 (Figs. 3 and 4) are then obtained utilizing F_1 . The uncertainties in F_1 and R are included in our total systematic error and in the error bands of our plots.

We have fitted the W dependence of our A_1 and A_2 data using an approach similar to that applied to unpolarized cross sections in Ref. [23], substituting for the DIS component a form based on the phenomenological spin structure parameterizations of Refs. [25, 26]. These fits served as input in the iterative procedure to obtain our radiative corrections and to calculate the integrals of g_1 and g_2 at constant Q^2 . Each spin asymmetry was fitted independently, since they represent different physical quantities.

To test quantitatively for global duality in g_1 , we can integrate in x over the resonance region and compare the results obtained from resonance data and DIS extrapolations (Fig. 3). We used our fit to integrate over the resonance region ($1.09 < W < 1.91$ GeV) and took the average of the integrals from several DIS extrapolations calculated from target mass corrected [27], next-to-leading order parton distribution functions (NLO PDFs) [28, 29, 30] over the same range of W at our average $Q^2 = 1.3$ GeV². We found the ratio of integrals, PDFs to data, to be 1.17 ± 0.08 , indicating agreement at only the two sigma level, and suggesting that PDF extrapolations into the resonance region may not be valid

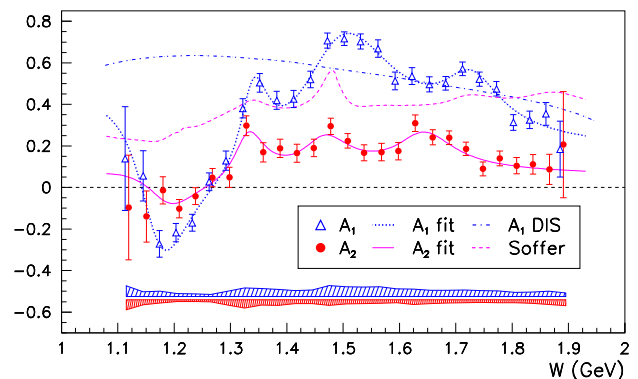


FIG. 2: Virtual photon asymmetries A_1 and A_2 from our data and corresponding fits. Also shown is the E155 fit to DIS data [25, 26], evaluated at our (x, Q^2) , and the Soffer limit for A_2 [31], based on our A_1 fit. The upper error band indicates the systematic error in A_1 , the lower one A_2 .

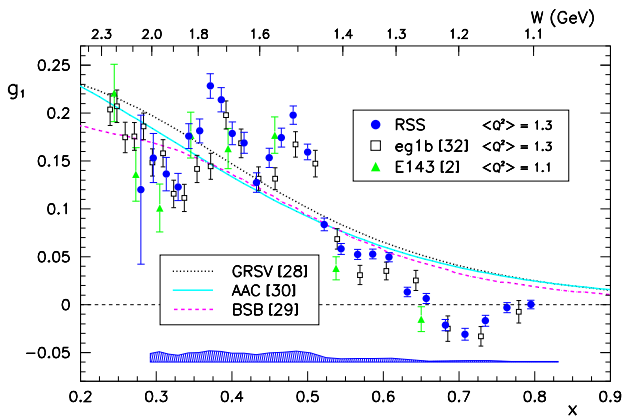


FIG. 3: Results for g_1 from this experiment (RSS) and other relevant data [2, 32], as well as target mass corrected NLO PDFs. The upper scale shows W (at $Q^2 = 1.3 \text{ GeV}^2$) for reference.

at this Q^2 . The ratios for restricted, but still rather broad, W ranges differ from unity by several sigmas, demonstrating that *local* polarized duality is not valid at our Q^2 : $1.09 < W < 1.4 \text{ GeV}$ is 6.47 ± 0.95 , and $1.4 < W < 1.91 \text{ GeV}$ is 0.87 ± 0.06 . Including also large x resummations for the PDFs [11], the global ratio changed to 1.42 ± 0.10 . The quoted errors are based on the data integrals only, including a 0.4% contribution from computing our fit at fixed Q^2 . Our results are in good agreement with the recent results from CLAS [13].

Approximate global duality within errors was reported by [10], based on A_1 resonance data averaged over a broad Q^2 range from 1.6 to 2.9 GeV^2 and compared to a DIS fit to data. The weak Q^2 dependence of A_1 (within large errors) allows for averaging, instead of calculating the ratio at each Q^2 value as is required for testing duality in the structure functions. But duality in the spin asymmetry $A_1 \propto g_1/F_1$ could be due to accidental cancellations in the ratio g_1/F_1 .

Our results for g_2 are much clearer, especially in the framework of the QCD OPE. The comparison of our data and the g_2^{ww} approximation, evaluated from our measurements of g_1 , provides strong evidence of the significance of higher-twist terms at this Q^2 , as shown in Fig. 4. Combining our measurements of g_1 and g_2 , we can investigate specifically the twist-3 contribution via the matrix element d_2 (Eq. 2). Over the measured range ($0.29 < x < 0.84$), we find $\overline{d_2} = 0.0057 \pm 0.0009$ (stat) ± 0.0007 (syst), including a 4% contribution to the systematic error from our fit's assumed Q^2 dependence. This significantly non-zero result highlights the limitation of leading-twist approximations. Extrapolating this result to $Q^2 = 5 \text{ GeV}^2$, assuming a $1/Q$ dependence, we find $\overline{d_2} = 0.0029$ compared to the SLAC result $d_2 = 0.0032 \pm 0.0017$ [33].

In summary, our results significantly increase the available information on the proton spin structure: These new

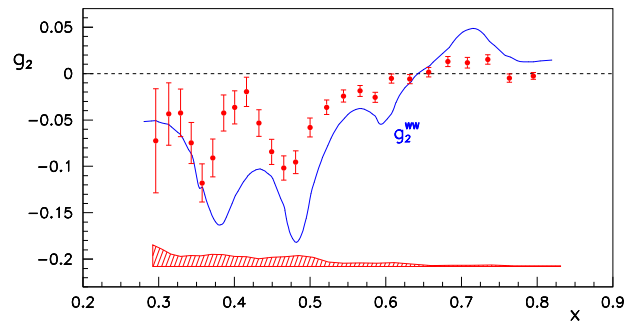


FIG. 4: Our (RSS) values for g_2 and the approximation g_2^{ww} (Eq. 1) as evaluated from our data.

data provide a connection to the measurements at DIS kinematics and fill a significant void in the explored regions. Our measurement with transverse spin arrangement is the first in the resonance region, with notably non-zero results. Our data clearly indicate the importance of higher twist contributions and thus quark–gluon correlations. We have established that Bloom-Gilman polarized duality is meaningful only for the resonance region as a whole, although local polarized duality may yet be observed at higher Q^2 ranges.

We would like to thank the Hall C technical staff and the accelerator operators for their efforts and dedication. This work was supported by the Department of Energy, the National Science Foundation, the Schweizerische Nationalfonds, and by the Institute of Nuclear and Particle Physics of the University of Virginia. The Southern Universities Research Association (SURA) operates the Thomas Jefferson National Accelerator Facility under contract for the United States Department of Energy.

-
- [1] J. Ashman et al. (EMC), Phys. Lett. B **206**, 364 (1988).
 - [2] K. Abe et al. (E143), Phys. Rev. Lett. **78**, 815 (1997); Phys. Rev. D **58**, 112003 (1998).
 - [3] D. Adams et al. (SMC), Phys. Lett. B **396**, 338 (1997).
 - [4] K. Ackerstaff et al. (HERMES), Phys. Lett. B **404**, 383 (1997), hep-ex/9703005.
 - [5] J. Kodaira, S. Matsuda, K. Sasaki, and T. Uematsu, Nucl. Phys. **B159**, 99 (1979).
 - [6] R. L. Jaffe, Comments Nucl. Part. Phys. **19**, 239 (1990).
 - [7] S. Wandzura and F. Wilczek, Phys. Lett. B **72**, 195 (1977).
 - [8] E. D. Bloom and F. J. Gilman, Phys. Rev. Lett. **25**, 1140 (1970); Phys. Rev. D **4**, 2901 (1971).
 - [9] W. Melnitchouk, R. Ent, and C. Keppel, Phys. Rept. **406**, 127 (2005), hep-ph/0501217.
 - [10] A. Airapetian et al. (HERMES), Phys. Rev. Lett. **90**, 092002 (2003), hep-ex/0209018.
 - [11] N. Bianchi, A. Fantoni, and S. Liuti, Phys. Rev. D **69**, 014505 (2004), hep-ph/0308057.
 - [12] Y. B. Dong, Phys. Lett. B **641**, 272 (2006).
 - [13] P. E. Bosted et al. (CLAS) (2006), submitted to Phys.

- Rev. C, hep-ph/0607283.
- [14] I. Niculescu et al., Phys. Rev. Lett. **85**, 1186 (2000).
 - [15] F. E. Close and N. Isgur, Phys. Lett. B **509**, 81 (2001), hep-ph/0102067.
 - [16] M. Hauger et al., Nucl. Instrum. Meth. **A462**, 382 (2001), nucl-ex/9910013.
 - [17] D. G. Crabb and D. B. Day, Nucl. Instrum. Meth. **A356**, 9 (1995).
 - [18] M. Steinacher and I. Sick, Nucl. Instrum. Meth. **A455**, 759 (2000).
 - [19] M. K. Jones et al. (RSS), Phys. Rev. C **74**, 035201 (2006), nucl-ex/0606015.
 - [20] J. W. Lightbody, Jr. and J. S. O'Connell, Computers in Physics **2**, 57 (1988).
 - [21] Y. Liang et al. (E94-110) (2004), nucl-ex/0410027.
 - [22] M. E. Christy, to be published.
 - [23] S. Stein et al., Phys. Rev. D **12**, 1884 (1975).
 - [24] I. Akushevich, A. Ilichev, N. Shumeiko, A. Soroko, and A. Tolkachev, Comput. Phys. Commun. **104**, 201 (1997), hep-ph/9706516.
 - [25] P. L. Anthony et al. (E155), Phys. Lett. B **493**, 19 (2000), hep-ph/0007248.
 - [26] F. R. Wesselmann, Ph.D. thesis, Old Dominion University (2000), SLAC-R-557.
 - [27] J. Blumlein and A. Tkabladze, Nucl. Phys. **B553**, 427 (1999), hep-ph/9812478.
 - [28] M. Gluck, E. Reya, M. Stratmann, and W. Vogelsang, Phys. Rev. D **53**, 4775 (1996), hep-ph/9508347.
 - [29] C. R. V. Bourrely, J. Soffer, and F. Buccella, Eur. Phys. J. **C41**, 327 (2005), hep-ph/0502180.
 - [30] Y. Goto et al. (Asymmetry Analysis), Phys. Rev. D **62**, 034017 (2000), hep-ph/0001046.
 - [31] J. Soffer and O. V. Teryaev, Phys. Lett. B **490**, 106 (2000), hep-ph/0005132.
 - [32] K. V. Dharmawardane et al. (CLAS), Phys. Lett. B **641**, 11 (2006), nucl-ex/0605028.
 - [33] P. L. Anthony et al. (E155), Phys. Lett. B **553**, 18 (2003), hep-ex/0204028.

APPENDIX

The results of our fits to A_1 and A_2 are detailed in table II and plotted against our data in figure 2. They are based on the method of Ref. [23], combining a number of Breit-Wigner shaped resonances BW_i and a deep-inelastic tail:

$$\text{fit} = \underbrace{\sum_{i=1}^4 BW_i}_{\text{Resonances}} + x^\alpha \underbrace{\sum_{n=0}^3 \beta_n x^n}_{\text{DIS}} \times \underbrace{\frac{1}{\sqrt{Q^2}}}_{A_2 \text{ only}}$$

where

$$BW_i = \frac{a_i \kappa_i^2 w_i^2 \Gamma_i \Gamma_i^\gamma}{\kappa_{cm}^2 [(w_i^2 - W^2)^2 + w_i^2 \Gamma_i^2]}$$

and

$$\Gamma_i = g_i \left(\frac{q_{cm}}{q_i} \right)^{(2l_i+1)} \left(\frac{q_i^2 + X_i^2}{q_{cm}^2 + X_i^2} \right)^{l_i}$$

$$\Gamma_i^\gamma = g_i \left(\frac{\kappa_{cm}}{\kappa_i} \right)^{(2j_i)} \left(\frac{\kappa_i^2 + X_i^2}{\kappa_{cm}^2 + X_i^2} \right)^{j_i}$$

with

$$\kappa_i = \sqrt{\frac{(w_i^2 + M^2 + Q^2)^2}{4w_i^2} - M^2}$$

$$q_i = \sqrt{\frac{(w_i^2 + M^2 - m_\pi^2)^2}{4w_i^2} - M^2}$$

$$\kappa_{cm} = \sqrt{\frac{(W^2 + M^2 + Q^2)^2}{4W^2} - M^2}$$

$$q_{cm} = \sqrt{\frac{(W^2 + M^2 - m_\pi^2)^2}{4W^2} - M^2}$$

We have optimized the values of amplitude a_i , centroid w_i , and width g_i of four Breit-Wigner resonances, as well as the exponent α and the polynomial coefficients β_n for the DIS tail. The values of the parameters X_i , l_i , and j_i were kept as in Ref. [23]. While the fits are a function of W , the DIS contribution is evaluated at the mean values of x and Q^2 of our data at that W bin.

In addition to the explicit contribution in the terms κ_i and κ_{cm} , and the indicated $1/\sqrt{Q^2}$ term for the DIS part of A_2 , our fit function depends on Q^2 via the interrelation of W , x and Q^2 :

$$W^2 = M^2 - Q^2 + \frac{Q^2}{x}$$

The resonance terms are otherwise Q^2 -independent.

TABLE II: Results of Fits to A_1 and A_2 , each based on 28 data points as plotted in figure 2.

Parameter	A_1 Fit	A_2 Fit
χ^2/dof	1.24	1.42
a_1	-0.562 ± 0.133	-0.147 ± 0.052
a_2	0.401 ± 0.069	0.220 ± 0.049
a_3	0.537 ± 0.042	0.158 ± 0.029
a_4	0.246 ± 0.044	0.173 ± 0.029
w_1	1.204 ± 0.010	1.214 ± 0.021
w_2	1.345 ± 0.005	1.338 ± 0.010
w_3	1.544 ± 0.012	1.479 ± 0.021
w_4	1.734 ± 0.009	1.653 ± 0.015
g_1	0.161 ± 0.065	0.137 ± 0.086
g_2	0.063 ± 0.025	0.071 ± 0.035
g_3	0.283 ± 0.058	0.113 ± 0.082
g_4	0.125 ± 0.043	0.129 ± 0.062
α	0.031 ± 0.391	0.458 ± 0.375
β_0	0.186 ± 0.074	0.100 ± 0.040
β_1	-0.032 ± 0.158	0.094 ± 0.079
β_2	-0.393 ± 0.272	-0.119 ± 0.133
β_3	0.957 ± 0.403	-0.025 ± 0.202

The choice of four resonances resulted in better fits than using only three, an option also supported by examining the second derivatives of the data smoothed with a spline curve. Additionally, the fits as reported here also gave excellent agreement with the cross sections $\sigma_{\text{TT}'}$ and $\sigma_{\text{LT}'}$ obtained from our data and a σ_{T} model [22].

Table III details the results of duality integral ratios for various sub-ranges (those matching the resonances assumes in our fit to A_1 , as well as those of [9]) and for the different PDFs [28, 29, 30]. The PDF integrals over individual resonances differed significantly from the data value, indicating that at our Q^2 , local duality is not observed in g_1^p .

TABLE III: Ratio of NLO PDFs to data, integrated over the indicated ranges. The top five W ranges are based on the location of the Breit-Wigner shapes resulting from our fit to A_1 and the last two match those of Ref. [9]; all are bounded by our acceptance. The elastic contribution [9] was calculated using the dipole form of the form factors.

	W Range	BSB	GRSV	AAC	Average
Delta	1.09-1.30GeV	3.41	4.18	3.96	3.93 ± 0.58
R1	1.30-1.39GeV	1.28	1.44	1.33	1.36 ± 0.10
R2	1.39-1.68GeV	0.77	0.82	0.75	0.78 ± 0.05
R3	1.68-1.79GeV	0.77	0.84	0.77	0.79 ± 0.06
Global	1.09-1.91GeV	1.11	1.23	1.14	1.17 ± 0.08
Delta + R1	1.09-1.40GeV	5.78	6.84	6.44	6.47 ± 0.95
R2 +	1.40-1.91GeV	0.84	0.91	0.84	0.87 ± 0.06